Raman Spectroscopic Characterization of Processed Human Dentin Biomaterials

ROBERT DŁUCIK[1], ALBERTO SCOGLIO[2,3,*], DOMENICO PUZZOLO[2], BARBARA TESTAGROSSA[2], LUCIA DENARO[2], ANGELA ALIBRANDI[4], ANTONIO TOSCANO[5], BOGUSŁAWA ORZECHOWSKA-WYLĘGAŁA[6], VALENTINA HARTWIG[7], GIUSEPPE ACRI[2]

[1]Dłucik Dental Clinic,
40-737 Katowice,
POLAND

[2]Department of Biomedical and Dental Sciences and Morphofunctional Imaging,
University of Messina,
98121 Messina,
ITALY

[3]IRCCS Centro Neurolesi "Bonino-Pulejo",
98121 Messina,
ITALY

[4]Department of Human Pathology in Adult and Developmental Age "Gaetano Barresi",
University of Messina,
98121 Messina,
ITALY

[5]U.O.S.D. Stroke Unit, Department of Clinical and Experimental Medicine,
University of Messina,
98121 Messina,
ITALY

[6]Children's Maxillofacial Surgery Clinic, Pediatric Surgery,
Medical University of Silesia,
40-752 Katowice,
POLAND

[7]Institute of Clinical Physiology,
CNR,
Via G. Moruzzi 1, 56124 Pisa,
ITALY

**Corresponding Author*

Abstract: - Processed dentin materials are increasingly investigated as bio-based scaffolds for regenerative dentistry due to their native collagen-mineral architecture and compositional similarity to bone tissue. Raman spectroscopy represents a valuable non-destructive approach for assessing the physicochemical organization of dentin, allowing the simultaneous evaluation of its mineral and organic components. This study aimed to characterize the Raman spectroscopic profile of human dentin samples prepared using three different commercial processing systems: BonMaker, Tooth Transformer, and Smart Dentin Grinder. Extracted teeth collected over different years and stored under controlled conditions were processed to evaluate the molecular features of the resulting dentin-derived biomaterials. Raman spectra were analyzed to derive specific spectroscopic indices describing the mineral-matrix balance and collagen matrix quality. These parameters were compared across the three processing technologies and against unprocessed dentin controls. The mineral

and collagen-related Raman indices suggested a substantial preservation of the principal organic matrix features across all samples, regardless of the storage period. Conversely, the observed spectral differences among the experimental groups appeared primarily related to the specific processing method applied by each device. These findings support the use of Raman spectroscopy as a robust and self-consistent tool for the structural and molecular characterization of dentinal-origin biomaterials. Overall, this technique provides a reliable analytical framework for defining the molecular fingerprint of processed dentin, supporting reproducible quality assessments of dentin-based regenerative matrices.

Key-Words: - dentin-derived biomaterials; Raman spectroscopy; collagen-mineral interface; physicochemical stability; regenerative dentistry; tooth-derived grafts; demineralized dentin matrix.

Received: March 27, 2026. Revised: April 22, 2026. Accepted: May 27, 2026. Published: October 1, 2026.

1 Introduction

Bone augmentation procedures are widely employed in implant dentistry to restore insufficient alveolar bone volume and ensure adequate support for implant placement and long-term functional stability [1], [2]. Various grafting strategies have been developed to improve bone regeneration and tissue integration.

Among regenerative biomaterials, dentin has increasingly attracted interest as an autologous graft material due to its compositional and structural similarities to bone tissue [3], [4]. Dentin is a mineralized hierarchical composite primarily composed of type I collagen and carbonated hydroxyapatite nanocrystals, whose interaction forms an organized collagen-mineral interface responsible for its mechanical properties and biological functionality [5], [6]. Previous investigations demonstrated that dentin-derived grafts can exhibit osteoconductive behavior while preserving native extracellular matrix components [4], [5], [6], [7].

Several studies have also suggested that dentin demineralization may facilitate the release of osteoinductive molecules entrapped within dentinal tubules, including bone morphogenetic proteins (BMPs) and growth factors involved in bone remodeling [7], [8]. Consequently, recent attention has focused on different dentin processing strategies such as BonMaker (BM), Tooth Transformer (TT), and Smart Dentin Grinder (SDG), which employ distinct preparation pathways capable of modifying the relative contribution of mineral and organic components [9], [10]. These processing approaches may generate grafts with different physicochemical characteristics and potentially influence their biological behavior and regenerative performance. However, despite the increasing use of these systems, only limited information exists regarding the molecular composition of processed dentin-derived biomaterials, and even fewer studies have investigated their long-term physicochemical stability during storage [10], [11].

Raman spectroscopy represents a promising analytical tool for addressing this gap. Raman spectroscopy is a vibrational spectroscopic technique based on the inelastic scattering of monochromatic light resulting from photon interactions with molecular vibrational modes. While most photons undergo elastic scattering (Rayleigh scattering), a small proportion exchanges energy with chemical bonds and generates Raman-shifted signals that provide molecular fingerprints of the analyzed material [12], [13].

Due to its chemical specificity and non-destructive nature, Raman spectroscopy has been extensively employed in several scientific fields including chemistry, materials science, geology, biology, and medicine [12], [13], [14], [15], [16]. In geology, it has been used for mineral identification and crystal characterization, whereas in biological and medical research it has been increasingly applied for tissue characterization, disease diagnosis, and biomarker identification [14], [15], [16].

In dentistry, Raman spectroscopy has emerged as a useful approach for studying dental hard tissues because it allows simultaneous assessment of mineral and organic components [17]. Several studies have employed Raman techniques to characterize enamel and dentin under different physiological and pathological conditions, including caries detection, demineralization-remineralization processes, adhesive-dentin interfaces, and biochemical alterations associated with tissue damage [18], [19], [20], [21], [22]. Raman-derived spectral parameters can provide information regarding phosphate content, carbonate substitution, collagen organization, mineral crystallinity, and mineral-to-matrix balance, thus allowing a detailed molecular characterization of dental tissues [18], [19], [20], [21].

An important advantage of Raman spectroscopy in dental biomaterial research is that it requires minimal sample preparation and enables simultaneous evaluation of both mineral and organic phases within a single acquisition [12], [17]. Such characteristics make Raman spectroscopy particularly suitable for studying hierarchical tissues such as dentin, where biological performance strongly depends on the integrity of the collagen-mineral interface.

However, despite its increasing application in dentistry, Raman spectroscopy has not yet been extensively employed to characterize processed dentin-derived biomaterials obtained using BM, TT, and SDG systems. In particular, information regarding long-term physicochemical preservation of these materials remains insufficient. Since prolonged storage may potentially affect the structural organization of the organic matrix and mineral phase, a spectroscopic evaluation of these changes may be relevant for understanding biomaterial stability and future clinical applicability [10].

Therefore, the aim of the present study was to evaluate the physicochemical stability of processed dentin-derived biomaterials following long-term storage through the identification of several indices by using Raman spectroscopy, with particular focus on the preservation of the organic matrix, mineral phase, and collagen-mineral interface.

2 Problem Formulation

2.1 Experimental Design and Sample Allocation

This in vitro study was designed to evaluate the physicochemical features of dentin-derived biomaterials obtained from extracted human teeth and processed using three different preparation systems. The experimental workflow was focused on the physical and molecular characterization of the mineral and organic components of dentin, with particular attention to the collagen-mineral interface. Extracted human teeth collected between 2018 and 2024 and stored under refrigerated conditions were used as experimental specimens. Freshly extracted teeth obtained in 2025 were used as control samples, representing native dentin without prolonged pre-processing storage. A total of 48 teeth, mainly extracted for periodontal indications, were included in the study. Except for the control samples, specimens were grouped according to the year of extraction and storage period. For each storage year, dentin specimens (six specimens per annual group) were further allocated to one of three processing systems: BonMaker (BM), Tooth Transformer (TT), and Smart Dentin Grinder (SDG).

The three processing systems were selected because they represent different technological approaches for preparing dentin-derived grafting materials, ranging from chemically modified dentin particles to mineral-preserving and minimally processed dentin matrices. Sample preparation and preliminary processing were performed at Dłucik Dental Clinic, Katowice, Poland. Raman spectroscopic analyses were carried out at the Department of Biomedical and Dental Sciences and Morphofunctional Imaging, University of Messina, Italy. All samples were anonymized before laboratory analysis and were used exclusively for in vitro research purposes.

2.2 Tooth Collection, Decontamination and Storage Conditions

After extraction, teeth were immediately immersed in 3% hydrogen peroxide solution for 3-5 min for preliminary surface decontamination. Each tooth was then mechanically cleaned under magnification to eliminate residual soft tissues, calculus, carious tissue, and restorative materials. Teeth previously subjected to endodontic treatment were excluded from the study to avoid potential confounding effects related to previous chemical or mechanical alteration of dentin. After cleaning, the specimens were re-immersed in 3% hydrogen peroxide for 5 min, dried using sterile gauze and compressed air, and placed in sealed sterilization pouches compliant with ISO 11607 standards. Each pouch was labeled according to the year of extraction and sample code. All the extracted teeth between 2018 and 2024 were stored at 4 °C until 2025, when they were retrieved from refrigerated conditions. Therefore, the refrigerated period discussed in this study refers to the pre-processing stage of the samples. No additional dehydration procedures were performed during storage. This approach was adopted to limit pre-analytical alterations of dentin hydration and to preserve the native organization of the collagen-mineral interface as much as possible before biomaterial preparation.

2.3 Generation of Dentin-Derived Particles

After sample retrieval, teeth were handled under standardized operative conditions. The specimens were briefly immersed again in 3% hydrogen peroxide for approximately 3 min for surface decontamination and then dried with sterile gauze.

Each tooth was mechanically fragmented using a sterile mortar and surgical hammer in order to obtain dentin fragments of heterogeneous size. This preliminary fragmentation step was performed to facilitate subsequent processing by the three dentin preparation devices while preserving the native composite architecture of the tissue.

The resulting dentin fragments were then processed according to the manufacturer's instructions for each system.

For the BonMaker system, dentin fragments were ground to obtain particles ranging approximately from 500 to 1000 µm. The particulate material was then subjected to an automated chemical demineralization protocol using hydrochloric acid (3.5-5%), ethanol (70%), and hydrogen peroxide (5%). The complete processing cycle lasted approximately 20 min and 50 s.

For the Tooth Transformer system, dentin fragments were crushed to obtain particles ranging approximately from 40 to 1200 µm. The material was processed through an automated cycle involving hydrogen peroxide, hydrochloric acid, demineralized water, and ultrasonic activation. The total processing time was approximately 25 min.

For the Smart Dentin Grinder system, dentin fragments were ground to obtain particles ranging approximately from 300 to 1300 µm. The resulting material was treated with a sodium hydroxide solution containing 20% ethanol and subsequently neutralized in phosphate-buffered saline. These three protocols were considered representative of different degrees of dentin modification, particularly in terms of mineral preservation, demineralization, exposure of the organic matrix, and modification of the mineral-to-collagen balance.

After processing, no additional manual sieving or particle-size selection was carried out. All samples were immediately prepared and transported under controlled conditions to the Health and Environmental Physics Laboratory of the University of Messina (Italy) for Raman spectroscopic analysis, which was performed immediately upon arrival

2.4 Raman Spectroscopy for Physical Characterization

Raman spectroscopy was used as a non-destructive analytical technique to characterize the molecular composition and physical organization of dentin-derived particles. BM, TT, SDG, and control dentin particles were investigated by Raman spectroscopy using a DXR SmartRaman spectrometer (Thermo Fisher Scientific, Waltham, MA, USA) equipped with a 785 nm diode laser as the excitation source. This analytical approach was selected because it allows the simultaneous evaluation of the mineral and organic components of dentin-derived materials without requiring extensive sample preparation or destructive procedures.

Before data collection, the spectrometer was calibrated according to the manufacturer's instructions using the wavelength calibration standards provided with the instrument. This preliminary step was performed to ensure spectral accuracy and reproducibility across all measurements. Raman spectra were acquired over a wavenumber interval ranging from 200 to 3200 cm^{-1}, thus covering both the fingerprint region and the high-wavenumber region associated with CH stretching vibrations. The spectral resolution was approximately 2 cm^{-1}.Laser irradiation was performed using an output power of 24 mW delivered through a 50 µm pinhole aperture. To obtain spectra with an adequate signal-to-noise ratio, each Raman spectrum was collected using 32 consecutive exposures, with an acquisition time of 30 s for each exposure. Therefore, the total acquisition time for each spectrum was 16 min.

Each sample was analyzed in dry state and in triplicate by obtaining the Raman spectrum from three different particles of the same sample, in order to improve the reliability and representativeness of the spectroscopic measurements. Before each acquisition, the dentin particles were repositioned within the sampling area. This procedure was adopted to reduce the influence of local heterogeneity and to account for possible spatial variations in the chemical composition and structural organization of the dentin-derived particles. The spectra obtained from repeated measurements were then used to generate representative spectral profiles for each sample.

All spectra were saved in .SPA format, and subsequent post-processing procedures were carried out using OMNIC software for dispersive Raman spectroscopy, version 9.0. During spectral post-processing, manual baseline correction was applied to each Raman spectrum in order to minimize background contributions and compensate for possible instrumental, optical, or sample-related variations. After baseline correction, the mean spectrum of each analyzed sample was calculated and used for subsequent comparative evaluations.

Raman spectra were then normalized using the vector normalization method previously reported in other studies [23], [24].

$$norm = \sqrt{(s_1^2 + s_2^2 + \cdots + s_n^2)} \quad (1)$$

Briefly, each intensity value of a given spectrum was divided by the corresponding Euclidean norm,

defined as the square root of the sum of the squared intensities across the entire spectrum (1). This procedure standardizes spectral intensity distributions and reduces variability related to differences in absolute signal intensity, sample positioning, and scattering efficiency. Particle size and surface morphology may affect Raman spectral quality, particularly absolute signal intensity, but the vector normalization of the spectra, the triplicate measurements, the sample repositioning, and the following calculation of intensity ratios contributed to reducing any potential source of variability related to the different particle sizes of the analyzed samples. The normalized spectra were therefore considered suitable for quantitative comparison among BM, TT, SDG, and control dentin samples.

2.5 Raman-Derived Indices

After baseline correction and spectral normalization, selected Raman intensity ratios were calculated and defined as Raman-derived indices to assess mineral-organic balance, collagen cross-linking, and collagen-related structural features of dentin-derived biomaterials. The Raman-derived indices were calculated using the following equations:

$$I_1 = \frac{I_{960}}{I_{1660}} \quad (2)$$

$$I_2 = \frac{I_{1065}}{I_{1450}} \quad (3)$$

$$I_3 = \frac{I_{2930}}{I_{430}} \quad (4)$$

$$I_4 = \frac{I_{1032}}{I_{1003}} \quad (5)$$

$$I_5 = \frac{I_{1660}}{I_{1242}} \quad (6)$$

$$I_6 = \frac{I_{1660}}{I_{1450}} \quad (7)$$

where I_v represents the normalized maximum Raman intensity of the band centered at the Raman shift $\tilde{v}$, expressed in cm^{-1}.

Mineral-organic balance indices:

Index 1 (I1)

I1 was calculated as the ratio between the phosphate band of hydroxyapatite at ~960 cm^{-1} and the collagen-related Amide I band at ~1660 cm^{-1}. This index was considered a mineral-to-matrix ratio [25], [26].

Index 2 (I2)

I2 was calculated as the ratio between the carbonate band of carbonated apatite at ~1065 cm^{-1} and the CH_2 band of the organic matrix at ~1450 cm^{-1}. This index was considered a carbonate-to-organic matrix ratio [27].

Index 3 (I3)

I3 was calculated as the ratio between the CH stretching band of the organic matrix at ~2930 cm^{-1} and the phosphate-related band of hydroxyapatite at ~430 cm^{-1}. This index was interpreted as a protein-to-mineral ratio [26], [27], [28].

Cross-linking:

Index 4 (I4)

I4 was calculated as the ratio between the pyridinium ring-related band at ~1032 cm^{-1} and the phenylalanine band at ~1003 cm^{-1}. This index was used as a marker of collagen cross-linking [29], [30].

Nature of collagen:

Index 5 (I5)

I5 was calculated as the ratio between the collagen-related Amide I band at ~1660 cm^{-1} and the Amide III band at ~1242 cm^{-1}. This index was associated with collagen organization [29].

Index 6 (I6)

I6 was calculated as the ratio between the collagen-related Amide I band at ~1660 cm^{-1} and the CH_2 band at ~1450 cm^{-1}. This index was associated with altered collagen quality [27], [30].

2.6 Statistical Analysis

Numerical data obtained from the ten Raman-derived indices were expressed as mean and standard deviation (SD). The normality of data distribution was assessed using the one-sample Kolmogorov-Smirnov test [31], [32]. Since the normal distribution showed a normal tendency (I1, $p = 0.379$; I2, $p = 0.486$; I3, $p = 0.353$; I4, $p = 0.932$; I5, $p = 0.237$; I6, $p = 0.774$), comparisons among the four groups, BM, TT, SDG and controls, were performed using one-way analysis of variance (ANOVA) [32]. When statistically significant differences were detected, pairwise comparisons were carried out using Tukey's honestly significant difference (HSD) post hoc test [33], [34]. Bonferroni correction was applied for multiple pairwise comparisons, and the adjusted significance threshold was set at $\alpha = 0.008$ (0.050/6). Statistical significance for the overall ANOVA was set at $p < 0.05$. Error-bar plots with 95% confidence intervals were generated to graphically represent group differences for each Raman index. Statistical analyses were performed using IBM SPSS Statistics for Windows, version 26.0 (IBM Corp., Armonk, NY, USA).

3 Problem Solution

3.1 Representative Raman Spectral Profile of Dentin-derived Biomaterials

All Raman spectra obtained from the different analyzed biomaterials (BM, TT, and SDG) and from the control group have shown the same spectral features.

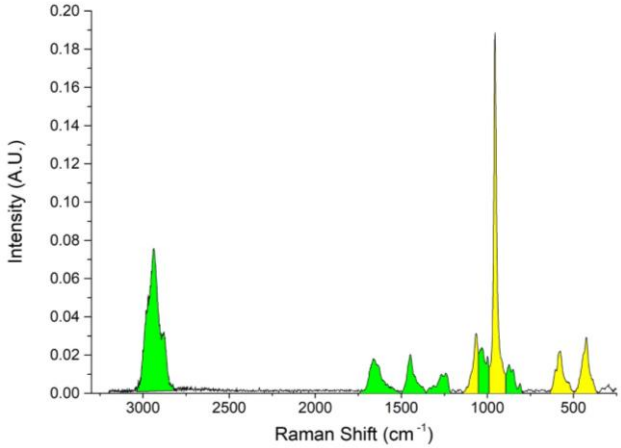

Fig. 1: Representative Raman spectral profile of dentin-derived material. Raman bands mainly related to the mineral phase of dentin are highlighted in yellow, while bands associated with the organic collagen/protein matrix are highlighted in green, allowing a visual overview of the main inorganic and organic contributions to the dentin Raman spectrum.
Source: created by the authors

Figure 1 shows a representative Raman spectrum of a dentin-derived biomaterial sample, selected to illustrate the main vibrational bands used for spectral assignment and Raman index calculation. The spectrum was acquired over the 200-3200 cm^{-1} range, which includes both the fingerprint region of mineralized dentin and the high-wavenumber region associated with organic matrix vibrations. In the figure, mineral bands are highlighted in yellow, while organic/collagen-related bands are highlighted in green.

The representative spectrum showed the typical Raman profile of dentin, with bands attributable to both the apatite mineral phase and the collagen-rich organic matrix. The principal mineral-related signals included phosphate and carbonate vibrations. These include the phosphate ν1 and ν2 bending modes, respectively, at approximately 430 and 590 cm^{-1}, the ν1 phosphate symmetric stretching peak at approximately 960 cm^{-1}, and the carbonate-related contribution at about 1065 cm^{-1}.

On the other hand, the organic component was mainly represented by collagen/protein-associated bands. These signals include proline and hydroxyproline bands at approximately 850 and 870 cm^{-1}, phenylalanine at 1003 cm^{-1}, Amide III at approximately 1242 cm^{-1}, CH_2 deformation at 1450 cm^{-1}, Amide I band at 1660 cm^{-1}, and CH-stretching vibrations at about 2930 cm^{-1}.

The detailed tentative assignment of the main Raman peaks and bands is reported in Table 1 (Appendix).

These spectral features were subsequently used to calculate Raman-derived indices describing the mineral-to-organic matrix balance, collagen cross-linking, and organic matrix organization in dentin-derived biomaterials.

3.2 Time-dependent Changes in Raman Indices

To assess time-dependent molecular changes associated with the duration of refrigerated storage of the samples prior to processing with BM, TT and SDG, six selected Raman-derived indices were evaluated across the 2018-2024 storage period. The indices were grouped into two functional categories: mineral-organic balance-related indices (Figure 2) and organic matrix-related indices (Figure 3).

Figure 2 shows the time-dependent behavior of the three indices, mainly reflecting the mineral-organic balance of the analyzed samples. In Figure 2a, the I1 index showed a substantially stable profile over time within each group. However, BM consistently exhibited lower values compared with TT, SDG, and control dentin, suggesting a reduced phosphate-to-amide I contribution and therefore a lower mineral-to-organic matrix ratio. TT showed intermediate values, whereas SDG remained closer to the control profile throughout the observation period.

A similar trend was observed for I2, corresponding to the 1065/1450 ratio (Figure 2b). This index remained relatively stable across the different years, without evidence of a progressive time-dependent decrease or increase. BM displayed persistently lower values compared with the other groups, while TT and SDG showed values more closely aligned with control dentin. This finding suggests that the carbonate-to-organic matrix balance was mainly influenced by the processing method rather than by the duration of storage.

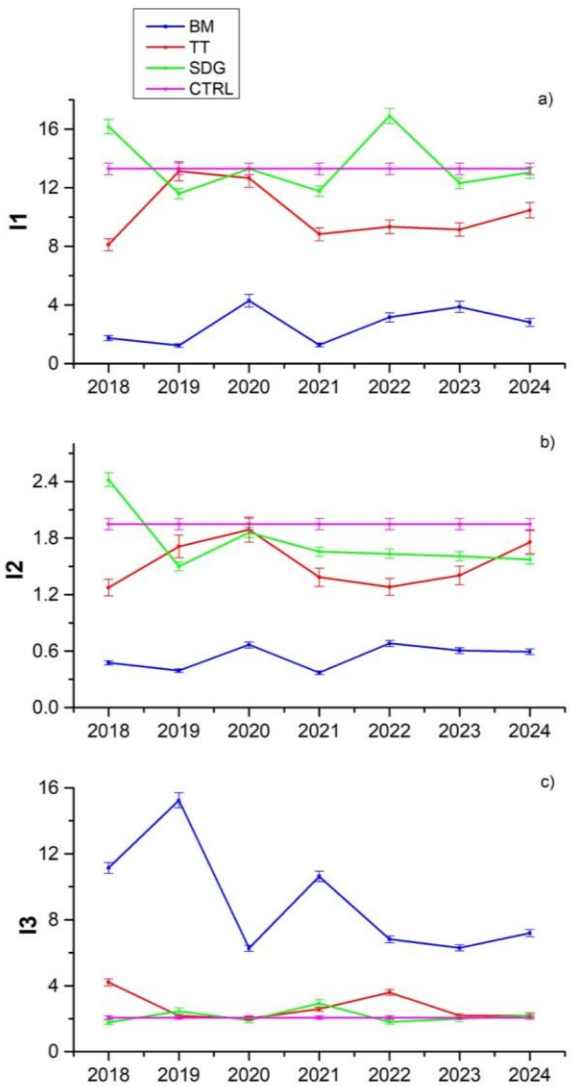

Fig. 2: Time-dependent behavior of mineral-organic balance-related Raman indices from 2018 to 2024. (a) I1: 960/1660 ratio; (b) I2: 1065/1450 ratio; (c) I3: 2930/430 ratio. BM: BonMaker; TT: Tooth Transformer; SDG: Smart Dentin Grinder; CTRL: Controls
Source: created by the authors

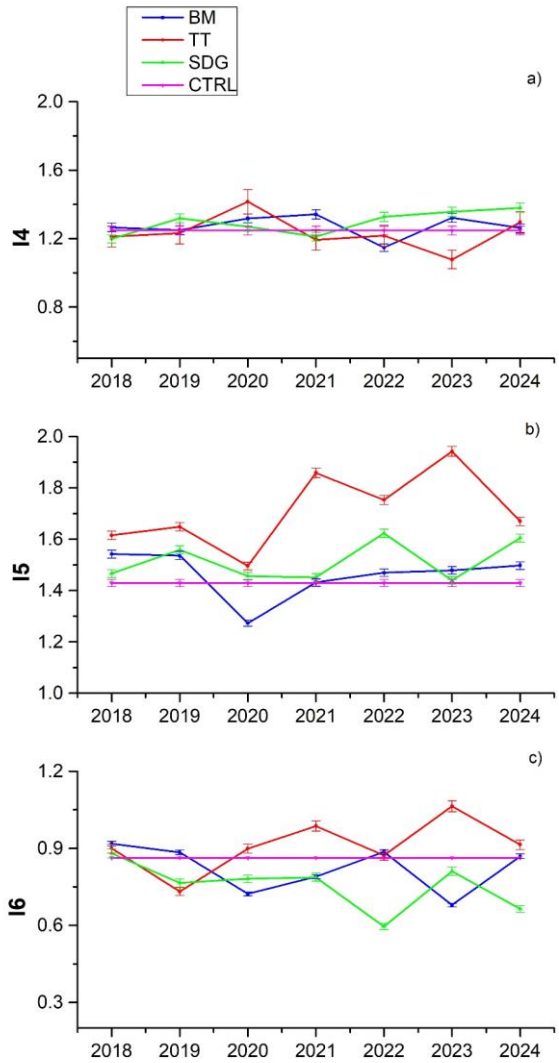

Fig. 3: Time-dependent behavior of organic matrix-related Raman indices from 2018 to 2024. (a) I4: 1032/1003 ratio; (b) I5: 1660/1242 ratio; (c) I6: 1660/1450 ratio. BM: BonMaker; TT: Tooth Transformer; SDG: Smart Dentin Grinder; CTRL: Controls
Source: created by the authors

The I3 index, reported in Figure 2c, showed the most evident separation between BM and the remaining groups. BM consistently displayed higher values across the entire storage period, indicating a greater relative contribution of the organic/protein component compared with the phosphate-related mineral signal. Particularly, BM values appeared higher in the earlier storage years and tended to decrease in more recent samples; however, this variation did not follow a strictly linear time-dependent pattern. Conversely, TT, SDG, and control dentin showed lower and more comparable values, with no clear evidence of progressive temporal alteration.

Figure 3 shows the time-dependent behavior of the three indices mainly associated with the organic matrix and collagen-related molecular features. In Figure 3a, the I4 index remained highly stable over time and showed only minor fluctuations among groups. No consistent divergence from the control profile was observed, suggesting preservation of the pyridinium/phenyl-related collagen signature during storage.

The I5 index, reported in Figure 3b, showed moderate intergroup variability but no clear progressive trend over time. TT generally exhibited higher values compared with BM, SDG, and control dentin, suggesting a distinct collagen organizational

profile associated with this processing method. However, the temporal distribution of this index did not indicate progressive collagen-related degradation during storage.

The I6 index (Figure 3c) showed limited temporal fluctuation across the analyzed years. Although some variability was observed among the different biomaterials, no consistent time-dependent pattern emerged. This suggests that the amide I/CH2-related collagen signature remained substantially preserved over the long-term storage period.

The time-course evaluation of the six Raman-derived indices indicates that long-term aging did not produce evident progressive changes in either mineral-organic balance or collagen-related molecular signatures. The main differences observed among BM, TT, SDG, and control dentin appeared to be primarily related to the specific processing protocols rather than to aging duration.

3.3 Statistical Analysis Results

Statistical analysis was performed to compare the distribution of the six selected Raman-derived indices among BM, TT, SDG, and control dentin samples. One-way ANOVA revealed significant intergroup differences ($p < 0.001$) for I1, I2, I3, I5, and I6, whereas I4 did not show significant differences among groups. Pairwise comparisons were then performed using the Tukey HSD post hoc test with Bonferroni correction (Table 2, Appendix).

For the mineral-organic balance-related indices, I1, I2, and I3 showed the most relevant intergroup differences. BM differed significantly from TT, SDG, and controls ($p < 0.001$) for all three indices, confirming a distinct Raman profile characterized by lower mineral-to-organic matrix ratios and a higher protein-to-mineral ratio. For I1, an additional significant difference was observed between TT and SDG, whereas no significant differences were detected between SDG and controls. For I2 and I3, TT, SDG, and controls were broadly comparable after correction. Lower I1 and I2 values and higher I3 values observed in BM suggest a reduced relative mineral contribution and a more extensive organic-related component, congruent with the more demineralized nature of this scaffold.

Regarding the organic matrix-related indices, I4 and I6 showed no robust pairwise differences after Bonferroni correction. In particular, I4 was not significant at the ANOVA level, while I6 showed only a global intergroup difference that was not confirmed by post hoc comparisons. Conversely, I5 showed significant differences mainly involving TT, which differed from BM and controls ($p < 0.001$) and SDG ($p = 0.005$), suggesting a distinct collagen organizational profile associated with this processing method. Despite we have not observed any significant difference for I4 among groups, it may be considered a positive result. The stability of I4 suggests that the collagen cross-linking signature was preserved across all the experimental groups. This could be explained by the presence of mature, pre-existing collagen cross-links in dentin, which were not altered during refrigerated storage.

Overall, the statistical analysis confirmed that the main molecular differences among groups were driven primarily by processing-dependent changes in the mineral-organic balance, particularly in BM. Collagen-related indices showed a more selective behavior, with I4 remaining stable, I5 distinguishing TT from the other groups, and I6 showing only a non-confirmed global trend.

The intergroup behavior of the selected Raman-derived indices was illustrated using error bar plots. Mean values were represented for each experimental group, and vertical bars indicated the corresponding 95% confidence intervals (Figure 4). This representation was used to better visualize the separation among BM, TT, SDG, and control dentin samples and to support the interpretation of the statistical comparisons reported in Table 2 (Appendix).

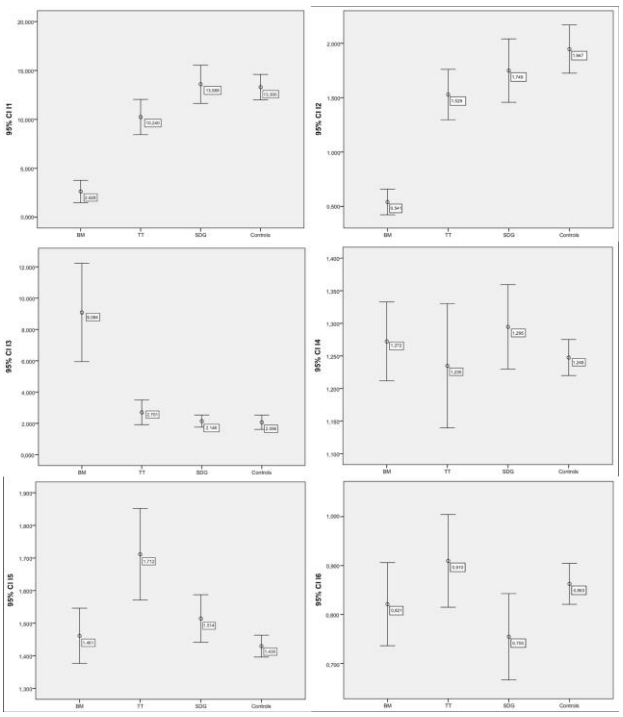

Fig. 4: Error-bar plots showing the mean ± standard deviation of the selected Raman spectroscopic indices across the analyzed groups and storage periods.

Source: created by the authors

4 Conclusion

The aim of the present study was to evaluate the physicochemical stability of dentin-derived biomaterials processed with BonMaker, Tooth Transformer, and Smart Dentin Grinder after storage, with particular attention to the preservation of the mineral phase, the organic matrix, and the collagen-mineral interface. Overall, the present findings suggest that storage time itself was not the main determinant of molecular change, whereas the processing protocol primarily shaped the biomaterial's spectroscopic profile. Biologically, this is relevant because the selected Raman indices interrogate complementary domains of dentin quality: I1 and I2 reflect the relative contribution of phosphate and carbonated apatite to the organic matrix, I3 reflects the protein-to-mineral balance, I4 provides an indication of collagen cross-link integrity, and I5-I6 are sensitive to collagen organization and matrix quality through the amide I, amide III, and CH_2 regions [17], [18], [25], [27], [28], [29], [30]. Within this framework, the BM profile, characterized by lower I1 and I2 together with higher I3, is most consistent with a more demineralized and matrix-exposed scaffold, indicating a shift away from the native dentin mineral-organic architecture and toward a collagen-richer graft material [3], [4], [7], [8], [9], [10]. By contrast, the greater similarity of SDG to native dentin suggests a better preservation of the original apatite-collagen balance and of the collagen-mineral interface, whereas TT appears to occupy an intermediate position; its higher I5 is more suggestive of collagen reorganization or altered secondary-structure packing than of overt collagen degradation [27], [29], [30]. The substantial stability of I4 across the storage period is also remarkable, as it argues against a major spontaneous loss of the mature collagen cross-link signature during refrigerated preservation. These findings indicate that the long-term biological identity of tooth-derived dentin grafts depends more on how dentin is processed than on how long it is stored under the present conditions.

More mineralized architecture, as observed in SDG-derived dentin particles, may provide a more rigid and stable scaffold contributing to maintaining graft volume longer. However, excessive mineralization could reduce the exposure and release of BMPs and other growth factors, potentially slowing the early phases of bone remodeling and regeneration. Therefore, preservation of the native dentin architecture may favor structural stability, but it does not necessarily mean superior osteoinductive or clinical performance. Since the present study wanted to physically characterize dentin-derived biomaterials and it did not directly evaluate bone formation, graft resorption, or implant osseointegration, these potential biological implications should be confirmed through histological and in vivo studies.

However, these findings may help clinicians to select the right biomaterial according to the bone defect. SDG could provide graft-volume maintenance, BM may improve the release of BMPs, while TT could represent a balance between structural stability and remodeling potential.

To the best of our knowledge, Raman studies specifically comparing BM, TT, and SDG and monitoring their storage-related stability remain very limited, making this study one of the first molecular-level investigations on this topic.

The main limitations are the lack of complementary ultrastructural, physicochemical, and biological analyses, such as SEM, FTIR or XRD, thermal or mechanical testing, and cell-based assays, which would have strengthened the interpretation of collagen quality, mineral crystallinity, and functional stability. Nevertheless, Raman spectroscopy remains highly attractive for regenerative dentistry because it enables rapid and non-destructive assessment of both mineral and organic components within the same acquisition, and may therefore represent a useful platform for quality control, stability monitoring, and protocol optimization of dentin-derived graft biomaterials.

Declaration of Generative AI and AI-assisted Technologies in the Writing Process

During the preparation of this work, the author(s) utilized artificial intelligence (AI) technologies solely for the purpose of linguistic refinement and grammatical correction. Following the application of these tools, the author(s) comprehensively reviewed, verified, and edited the resulting text. The author(s) maintain full accountability and responsibility for the accuracy, integrity, and final content of the publication.

References:

[1] Buser D, Urban I, Monje A, Kunrath MF, Dahlin C, Guided bone regeneration in implant dentistry: Basic principle, progress over 35 years, and recent research activities, *Periodontology 2000*, Vol.93, No.1, 2023, pp. 9–25. https://doi.org/10.1111/prd.12539.

[2] Wang B, Feng C, Liu Y, Mi F, Dong J, Recent advances in biofunctional guided bone regeneration materials for repairing defective alveolar and maxillofacial bone: A review, *Japanese Dental Science Review*, Vol.58, 2022, pp. 233–248. https://doi.org/10.1016/j.jdsr.2022.07.002.

[3] Gual-Vaqués P, Polis-Yanes C, Estrugo-Devesa A, Ayuso-Montero R, Marí-Roig A, López-López J, Autogenous teeth used for bone grafting: A systematic review, *Medicina Oral, Patología Oral y Cirugía Bucal*, Vol.23, No.1, 2018, pp. e112–e119. https://doi.org/10.4317/medoral.22197.

[4] Inchingolo AM, Malcangi G, Inchingolo AD, et al., Autologous tooth-derived biomaterials in alveolar bone regeneration: A systematic review of clinical outcomes and histological evidence, *Journal of Functional Biomaterials*, Vol.16, No.10, 2025, Article 367. https://doi.org/10.3390/jfb16100367.

[5] Ulian G, Moro D, Valdrè G, Hydroxyapatite and related minerals in bone and dental tissues: Structural, spectroscopic and mechanical properties from a computational perspective, *Biomolecules*, Vol.11, No.5, 2021, Article 728. https://doi.org/10.3390/biom11050728.

[6] Yu L, Wei M, Biomineralization of collagen-based materials for hard tissue repair, *International Journal of Molecular Sciences*, Vol.22, No.2, 2021, Article 944. https://doi.org/10.3390/ijms22020944.

[7] Gao X, Qin W, Wang P, Wang L, Weir MD, Reynolds MA, Zhao L, Lin Z, Xu HHK, Nano-structured demineralized human dentin matrix to enhance bone and dental repair and regeneration, *Applied Sciences*, Vol.9, No.5, 2019, Article 1013. https://doi.org/10.3390/app9051013.

[8] Lee B, Choi H, Sohn DS, Optimizing bone regeneration with demineralized dentin-derived graft material: Impact of demineralization duration in a rabbit calvaria model, *Journal of Functional Biomaterials*, Vol.15, No.11, 2024, Article 331. https://doi.org/10.3390/jfb15110331.

[9] Minetti E, Berardini M, Corbella S, Taschieri S, New classification of autologous tooth-derived grafting materials: Fundamental concepts, *International Journal of Dentistry*, Vol.2025, 2025, Article 6646405. https://doi.org/10.1155/IJOD/6646405.

[10] Dłucik R, Orzechowska-Wylęgała B, Dłucik D, et al., Comparison of clinical efficacy of three different dentin matrix biomaterials obtained from different devices, *Expert Review of Medical Devices*, Vol.20, No.4, 2023, pp. 313–327. https://doi.org/10.1080/17434440.2023.2190512.

[11] Dłucik R, Scoglio A, Puzzolo D, Testagrossa B, Alibrandi A, Toscano A, Orzechowska-Wylęgała B, Acri G, Physicochemical stability of dentin-derived biomaterials during long-term storage, *Journal of Functional Biomaterials*, Vol.17, No.6, 2026, Article 284. https://doi.org/10.3390/jfb17060284.

[12] Jones RR, Hooper DC, Zhang L, Wolverson D, Valev VK, Raman techniques: Fundamentals and frontiers, *Nanoscale Research Letters*, Vol.14, 2019, Article 231. https://doi.org/10.1186/s11671-019-3039-2.

[13] Geraldes CFGC, Introduction to infrared and Raman-based biomedical molecular imaging and comparison with other modalities, *Molecules*, Vol.25, No.23, 2020, Article 5547. https://doi.org/10.3390/molecules25235547.

[14] Nasdala L, Schmidt C, Applications of Raman spectroscopy in mineralogy and geochemistry, *Elements*, Vol.16, No.2, 2020, pp. 99–104. https://doi.org/10.2138/gselements.16.2.99.

[15] Chandra A, Kumar V, Garnaik UC, Dada R, Qamar I, Goel VK, Agarwal S, Unveiling the molecular secrets: A comprehensive review of Raman spectroscopy in biological research, *ACS Omega*, Vol.9, No.51, 2024, pp. 50049–50063. https://doi.org/10.1021/acsomega.4c00591.

[16] Auner GW, Koya SK, Huang C, et al., Applications of Raman spectroscopy in cancer diagnosis, *Cancer and Metastasis Reviews*, Vol.37, 2018, pp. 691–717. https://doi.org/10.1007/s10555-018-9770-9.

[17] Otel I, Overall review on recent applications of Raman spectroscopy technique in dentistry, *Quantum Beam Science*, Vol.7, No.1, 2023, Article 5. https://doi.org/10.3390/qubs7010005.

[18] Sarna-Boś K, Boguta P, Szymańska-Chargot M, Skic K, Zdunek A, Stachurski P, et al., Insight into structural and chemical profile/composition of powdered enamel and dentine in different types of permanent human teeth, *Micron*, Vol.179, 2024, Article 103608. https://doi.org/10.1016/j.micron.2024.103608.

[19] Almahdy A, Downey FC, Sauro S, Cook RJ, Sherriff M, Richards D, Watson TF, Banerjee A, Festy F, Microbiochemical analysis of carious dentine using Raman and fluorescence spectroscopy, *Caries Research*, Vol.46, No.5, 2012, pp. 432–440. https://doi.org/10.1159/000339487.

[20] Alturki M, Koller G, Warburton F, Almhöjd U, Banerjee A, Biochemical characterisation of carious dentine zones using Raman

spectroscopy, *Journal of Dentistry*, Vol.105, 2021, Article 103558. https://doi.org/10.1016/j.jdent.2020.103558.

[21] Timchenko EV, Timchenko PE, Volova LT, Frolov OO, Zibin M, Bazhutova IV, Raman spectroscopy of changes in the tissues of teeth with periodontitis, *Diagnostics*, Vol.10, No.11, 2020, Article 876. https://doi.org/10.3390/diagnostics10110876.

[22] Toledano M, Osorio E, Aguilera FS, Cabello I, Toledano-Osorio M, Osorio R, Ex vivo detection and characterization of remineralized carious dentin by nanoindentation and single point Raman spectroscopy after amalgam restoration, *Journal of Raman Spectroscopy*, Vol.48, 2017, pp. 384–392. https://doi.org/10.1002/jrs.5055.

[23] Gautam R, Vanga S, Ariese F, Umapathy S, Review of multidimensional data processing approaches for Raman and infrared spectroscopy, *EPJ Techniques and Instrumentation*, Vol.2, 2015, Article 8. https://doi.org/10.1140/epjti/s40485-015-0018-6.

[24] Acri G, Testagrossa B, Scoglio A, Attanzio A, Arfuso F, Rizzo M, Piccione G, Giannetto C, Alternative methodology for cortisol evaluation before and after sheep shearing using Raman spectroscopy: A feasibility study, *Animals*, Vol.15, No.19, 2025, Article 2776. https://doi.org/10.3390/ani15192776.

[25] Seyedmahmoud R, McGuire JD, Wang Y, Thiagarajan G, Walker MP, The interrelationship of microstructure and hardness of human coronal dentin using reference point indentation technique and micro-Raman spectroscopy, *Dental Materials*, Vol.33, No.10, 2017, pp. 1069–1074. https://doi.org/10.1016/j.dental.2017.07.005.

[26] Douchy L, Gauthier R, Abouelleil-Sayed H, Colon P, Grosgogeat B, Bosco J, The effect of therapeutic radiation on dental enamel and dentin: A systematic review, *Dental Materials*, Vol.38, No.7, 2022, pp. e181–e201. https://doi.org/10.1016/j.dental.2022.04.014.

[27] Salehi H, Terrer E, Panayotov I, Levallois B, Jacquot B, Tassery H, Cuisinier F, Functional mapping of human sound and carious enamel and dentin with Raman spectroscopy, *Journal of Biophotonics*, Vol.6, No.10, 2013, pp. 765–774. https://doi.org/10.1002/jbio.201200095.

[28] Reed R, Xu C, Liu Y, Gorski JP, Wang Y, Walker MP, Radiotherapy effect on nano-mechanical properties and chemical composition of enamel and dentine, *Archives of Oral Biology*, Vol.60, No.5, 2015, pp. 690–697. https://doi.org/10.1016/j.archoralbio.2015.02.020.

[29] Toledano M, Aguilera FS, Osorio E, Cabello I, Toledano-Osorio M, Osorio R, Functional and molecular structural analysis of dentine interfaces promoted by a Zn-doped self-etching adhesive and an in vitro load cycling model, *Journal of the Mechanical Behavior of Biomedical Materials*, Vol.50, 2015, pp. 131–149. https://doi.org/10.1016/j.jmbbm.2015.05.026.

[30] Toledano M, Osorio E, Osorio MT, Aguilera FS, Toledano R, Fernández-Romero E, Osorio R, Dexamethasone-doped nanoparticles improve mineralization, crystallinity and collagen structure of human dentin, *Journal of Dentistry*, Vol.130, 2023, Article 104447. https://doi.org/10.1016/j.jdent.2023.104447.

[31] Ghasemi A, Zahediasl S, Normality tests for statistical analysis: A guide for non-statisticians, *International Journal of Endocrinology and Metabolism*, Vol.10, No.2, 2012, pp. 486–489. https://doi.org/10.5812/ijem.3505.

[32] Mishra P, Pandey CM, Singh U, Gupta A, Sahu C, Keshri A, Descriptive statistics and normality tests for statistical data, *Annals of Cardiac Anaesthesia*, Vol.22, No.1, 2019, pp. 67–72. https://doi.org/10.4103/aca.ACA_157_18.

[33] Tukey JW, Comparing individual means in the analysis of variance, *Biometrics*, Vol.5, No.2, 1949, pp. 99–114. https://doi.org/10.2307/3001913.

[34] Avcı H, Dağ O, A comprehensive Monte Carlo simulation study on multiple comparison methods after ANOVA, *Journal of Advanced Research in Natural and Applied Sciences*, Vol.10, No.3, 2024, pp. 493–505. https://doi.org/10.28979/jarnas.1429315.

[35] Wang Y, Spencer P, Quantifying adhesive penetration in adhesive/dentin interface using confocal Raman microspectroscopy, *Journal of Biomedical Materials Research*, Vol.59, No.1, 2002, pp. 46–55. https://doi.org/10.1002/jbm.1215.

APPENDIX

Table 1. Assignment of the main Raman bands and peaks detected in dentin and their associated biochemical components

Raman Shift (cm^{-1})	Assignment	Biochemical Component	Reference
430	ν_2 PO_4^{3-} bending	Phosphate (apatite)	[35]
590	ν_4 PO_4^{3-} bending	Phosphate (apatite)	[35]
850	C–C stretching vibration of proline	Collagen	[20], [35]
870	C–C stretching vibration of hydroxyproline	Collagen	[20], [35]
960	ν_1 PO_4^{3-} symmetric stretching	Phosphate (apatite)	[35]
1003	Phenylalanine ring breathing	Protein / collagen matrix	[22]
1032	C–C vibration of the pyridinium ring	Collagen cross-linking	[28], [29]
1065	ν_1 CO_3^{2-} substitution/C–O stretching	Carbonate (apatite)	[27]
1242–1270	Amide III / C-N stretching and N-H bending	Collagen	[20], [35]
1450	CH_2 deformation/CH wagging	Organic matrix	[35]
1660	Amide I/ C=O stretching	Collagen (secondary structure)	[35]
2930	CH stretching	Organic matrix	[20], [28], [35]

Source: created by the authors

Table 2. Pairwise comparisons among experimental groups for the six selected Raman-derived indices (Tukey HSD post hoc test with Bonferroni correction). Significant values ($p < 0.008$) are indicated with *

	I1	I2	I3	I4	I5	I6
BM vs. TT	<0.001*	<0.001*	<0.001*	0.766	<0.001*	0.251
BM vs. SDG	<0.001*	<0.001*	<0.001*	0.937	0.747	0.490
BM vs. Ctrl	<0.001*	<0.001*	<0.001*	0.917	0.930	0.807
TT vs. SDG	0.006*	0.347	0.936	0.423	0.005*	0.013
TT vs. Ctrl	0.014	0.018	0.908	0.987	<0.001*	0.743
SDG vs. Ctrl	0.989	0.441	0.999	0.619	0.392	0.119

Source: created by the authors

Contribution of individual authors to the creation of a scientific article (ghostwriting policy)

- Robert Dłucik collected and prepared the clinical samples.
- Domenico Puzzolo managed samples, prepared the figures, and supervised the manuscript.
- Alberto Scoglio performed the Raman spectroscopy experiments, wrote the original paper, and prepared the figures.
- Barbara Testagrossa performed the Raman spectroscopy analysis.
- Lucia Denaro analyzed the data.
- Angela Alibrandi performed the statistical analysis.
- Antonio Toscano critically revised the manuscript.
- Orzechowska-Wylęgała Bogusława contributed to the clinical interpretation of the results.
- Valentina Hartwig contributed to manuscript preparation.
- Giuseppe Acri supervised the research, wrote the original paper and prepared the figures.

Sources of funding for research presented in a scientific article or scientific article itself

This research received no external funding.

Conflict of Interest

The authors declare no conflicts of interest

Creative Commons Attribution License 4.0 (Attribution 4.0 International, CC BY 4.0)

This article is published under the terms of the Creative Commons Attribution License 4.0
https://creativecommons.org/licenses/by/4.0/deed.en_US